FLCN, a novel autophagy component, interacts with GABARAP and is regulated by ULK1 phosphorylation

Elaine A. Dunlop[1], Sara Seifan[1], Tijs Claessens[1,2], Christian Behrends[3], Miriam A.F. Kamps[2], Ewelina Rozycka[4], Alain J. Kemp[5], Ravi K. Nookala[6], John Blenis[7], Barry J. Coull[2], James T. Murray[4,8], Maurice A.M. van Steensel[2,9], Simon Wilkinson[5] and Andrew R. Tee[1]

[1]Institute of Cancer and Genetics, Cardiff University, Heath Park, Cardiff, Wales, CF14 4XN, UK.

[2]Department of Dermatology, GROW School for Oncology and Developmental Biology, Maastricht University Medical Center, PO Box 5800, 6202 AZ Maastricht, Netherlands.

[3]Frankfurt Institute for Molecular Life Sciences (FMLS) and Institute of Biochemistry II, Goethe University School of Medicine, Frankfurt, Germany.

[4]Centre for Cancer Research and Cell Biology, School of Medicine, Dentistry and Biomedical Science, Queen's University Belfast, 97 Lisburn Road, Belfast, BT9 7BL, UK.

[5]Institute of Genetics and Molecular Medicine, Edinburgh Cancer Research UK Centre, University of Edinburgh, Crewe Road South, Edinburgh, EH4 2XR, UK.

[6]Dept of Biochemistry, University of Cambridge, Tennis Court Road, Cambridge CB2 1GA, UK.

[7]Department of Cell Biology, Harvard Medical School, 240 Longwood Ave, Boston, MA , USA.

[8]Trinity Biomedical Sciences Institute, School of Biochemistry and Immunology, Trinity College Dublin, Ireland

[9]Immunos, Institute of Medical Biology, Singapore

To whom correspondence should be addressed: Dr. Andrew R. Tee, Institute of Cancer and Genetics, Cardiff University, Cancer Genetics Building, 1st Floor, Heath Park, Cardiff, CF14 4XN, UK. Tel.: +44 2920 687856; Fax: +44 2920 746551; E-mail: teea@cardiff.ac.uk

Running title**:** *FLCN is a novel regulator of autophagy*

Conflict of Interest

The authors declare no conflict of interest and have no financial disclosures to make.

Abbreviations

AMPK - AMP-dependent protein kinase; ATG - autophagy-related; BHD - Birt-Hogg-Dubé; FLCN - folliculin; FNIP - FLCN interacting protein; GABARAP - γ-aminobutyric acid receptor-associated protein; GATE-16 - Golgi-associated ATPase enhancer of 16 kDa; GST - glutathione S-transferase; KRB - Kreb's Ringer Buffer; MAP1LC3 - microtubule-associated protein 1 light chain 3; LIR - LC3-interacting region; MBP - myelin basic protein; mTORC1 - mechanistic target of rapamycin complex 1; PE - phosphatidylethanolamine; SQSTM1 - sequestome 1; TGFβ - transforming growth factor beta; ULK1 - Unc-51 like kinase.

Abstract

Birt-Hogg-Dubé (BHD) syndrome is a rare autosomal dominant condition caused by mutations in the *FLCN* gene and characterised by benign hair follicle tumours, pneumothorax and renal cancer. Folliculin (FLCN), the protein product of the *FLCN* gene, is a poorly characterised tumour suppressor protein, currently linked to multiple cellular pathways. Autophagy maintains cellular homeostasis by removing damaged organelles and macromolecules. Although the autophagy kinase, ULK1, is known to drive autophagy, the mechanisms are not fully elucidated and few ULK1 substrates have been identified to date. Here, we identify that loss of FLCN moderately impairs basal autophagic flux, while re-expression of FLCN rescues autophagy. We reveal that FLCN is a new substrate of ULK1 and elucidate three novel ULK1-mediated phosphorylation sites (Ser406, Ser537 and Ser542) within FLCN. In addition to ULK1-mediated phosphorylation of FLCN, our findings demonstrate that FLCN interacts with a second integral component of the autophagy machinery, GABARAP. The FLCN-GABARAP association is modulated by the presence of either FNIP1 or FNIP2. This FLCN-GABARAP interaction is further regulated by ULK1, through ULK1 phosphorylation of FLCN. As observed by elevation of GABARAP, SQSTM1 and LC3 in chromophobe and clear cell tumours from a BHD patient, we uncover that autophagy is impaired in BHD-associated renal tumours. Consequently, this work reveals a novel facet of autophagy regulation by ULK1 and substantially contributes to our understanding of FLCN function by linking it directly to autophagy through GABARAP and ULK1.

Keywords: Autophagy, FLCN, ULK1, GABARAP, BHD, SQSTM1, LC3B

Introduction

Macroautophagy (hereafter referred to as autophagy) is an evolutionarily conserved process where intracellular lipid and protein components are broken down to replenish cellular energy and amino acid supplies. Autophagy also removes protein aggregates, redundant macromolecules and dysfunctional organelles that, if not efficiently recycled, contribute to cell stress and consequently disease.[1] For example, autophagy plays both pro- and anti-oncogenic roles in cancer development (for a review see ref. 1), while defects result in age-related cardiomyopathy[2] and can lead to marked neurodegeneration.[3,4] Autophagy involves sequestering cytoplasmic material in double-membraned vesicles known as autophagosomes, which subsequently fuse with lysosomes to form autolysosomes. Once fusion occurs, lysosomal hydrolases degrade sequestered material allowing permeases to transport amino acids and lipids into the cytoplasm for use in either biosynthesis or the generation of energy (for a review see ref. 5).

Yeast screens uncovered over 30 autophagy-related (*ATG*) genes,[6] many of which are recruited to the phagophore assembly site, a pre-autophagosomal membrane structure. ATG8 is conjugated to phosphatidylethanolamine (PE) and selectively incorporated into autophagosomes, making it a commonly used autophagy marker. Mammals have two ATG8 subfamilies, the microtubule-associated protein 1 light chain 3 (MAP1LC3, commonly called LC3) subgroup and the γ-aminobutyric acid receptor-associated protein (GABARAP)/Golgi-associated ATPase enhancer of 16 kDa (GATE-16) subfamily. Both mammalian ATG8 subfamilies are modified by PE conjugation, localise to autophagosomes[7] and are essential for autophagy. Current evidence indicates that LC3 and GABARAP act at different stages of autophagosome formation.[8]

The Unc-51 like kinase (ULK1) (the mammalian equivalent of Atg1) acts at the most upstream step of autophagy.[9] ULK1 is a serine/threonine kinase that functions within a complex containing ATG13,

FIP200 and ATG101 to drive autophagosome formation.[10-13] This kinase complex is positively regulated by many internal ULK1-mediated phosphorylation events, including ULK1 autophosphorylation.[10-12, 14] In addition, when energy and nutrients are plentiful, the mechanistic target of rapamycin complex 1 (mTORC1) promotes cell growth in part by inhibiting autophagy via phosphorylation of ULK1.[10,11] Conversely, during energy and nutrient stress when cell growth is not feasible, AMP-dependent protein kinase (AMPK) interacts with and phosphorylates ULK1 to enhance autophagy.[15-18] Downstream ULK1 substrates have remained largely elusive. AMBRA1 was the first ULK1 substrate identified that is integral to the autophagy machinery[19] but is not a component of the ULK1-ATG13-FIP200 complex. More recently, ULK1 phosphorylation of ATG9 has been identified as an important step during expansion of the isolation membrane.[20] ULK1 is known to indirectly impact autophagy via phosphorylation of both AMPK [21] and Raptor within mTORC1.[22,23]

Mutations in *FLCN* are responsible for Birt-Hogg-Dubé (BHD) syndrome (MIM #135150), characterised by benign hair follicle tumours, pneumothorax, cysts and renal cancer.[24] BHD is a ciliopathy and FLCN is localised at primary cilia.[25] Interestingly, a compromised ability to activate autophagy has been hypothesised to underlie some ciliopathies,[26] raising the possibility that autophagy may be altered in BHD syndrome. In support of this autophagy connection, FLCN was recently shown to localise to lysosomes and modulate nutrient sensing through the Rag small G proteins.[27-29] Given these findings, we wanted to ascertain whether autophagy is compromised in BHD syndrome. Our study uncovers a link between autophagy and BHD syndrome, revealing that FLCN is an important component of the autophagy machinery and is a downstream substrate of ULK1.

Results

Loss of FLCN affects SQSTM1 expression - Sequestome-1 (SQSTM1, also known as p62) is an established marker of autophagy, which associates with autophagosomes and is degraded during autophagy.[30] Of interest, SQSTM1 is often amplified in renal cell carcinoma.[31] Given that BHD syndrome predisposes patients to renal cell carcinoma, we analysed whether *FLCN* loss could enhance SQSTM1 protein levels. Previously, it was observed that tumour initiation via cystogenesis occurred within *Flcn* +/- mice upon loss of *Flcn* in renal proximal tubule cells.[32] Therefore, we utilised human renal proximal tubule (HK2) cells with stable *FLCN* knockdown for our studies. We observed higher endogenous SQSTM1 protein expression in *FLCN*-deficient cells compared to control cells, which was more pronounced under normal growth conditions (Fig. 1A), implying FLCN may play a role in basal autophagy, but may be dispensable for acute starvation-induced autophagy. We also observed a similar pattern in $Flcn^{-/-}$ mouse embryonic fibroblasts (MEFs) (Fig. S1A). We then re-expressed FLCN in *FLCN*-deficient HK2 cells under normal growth conditions and co-expressed HA-SQSTM1 to specifically measure autophagy in the transfected cells. As indicated by reduced SQSTM1, re-expression of FLCN restored a higher level of basal autophagy (Fig. 1B). Immunohistochemistry revealed elevated SQSTM1 protein levels in a BHD patient renal tumour (with a c.499C>T mutation encoding a truncated FLCN mutant, pGln167X) when compared to unaffected tissue (Fig. 1C). Collectively, this data reveals that the protein expression of SQSTM1 is negatively regulated by FLCN.

FLCN-deficient cells exhibit impaired autophagy – We wanted to examine whether this elevation of SQSTM1 protein might be due to autophagy defects in the *FLCN*-deficient cells. We assessed autophagic flux using a vector expressing tandem red and green fluorescent protein-tagged LC3 (RFP-GFP-LC3), which works on the principle that the GFP signal is less stable in the acidic environment of the lysosome than the RFP signal.[33] Of the cells displaying multiple puncta under normal growth conditions, we detected proportionally fewer red puncta in the *FLCN* knockdown HK2 cells (Fig. 2A-B), indicating impaired maturation of autophagosomes (reduced fusion of autophagosomes with lysosomes), and

therefore reduced autophagic flux. This fits with our finding of SQSTM1 accumulation due to lack of degradation in lysosomes. Interestingly, in both HK2 cells (Fig. 2C) and HEK293 cells (Fig. 2D) *FLCN* knockdown causes a reduction in LC3B-II conversion following chloroquine treatment. As perturbation of autophagosome maturation would be expected to allow an accumulation of LC3B-II, this suggests that autophagosome synthesis may also be modestly impaired in *FLCN*-deficient cells. Analysis of another mammalian ATG8 orthologue, GABARAP, which has a potential role in regulating the sealing process needed for autophagosome maturation,[8] revealed enhanced endogenous GABARAP expression in both *FLCN*-deficient HK2 and HEK293 cells (Fig. 2C-D). This elevation of GABARAP protein was not due to enhanced *GABARAP* gene expression, as mRNA levels were comparable between the cell lines (Fig. S1B). Overall, this data indicates an impaired autophagy pathway operates in the absence of FLCN, along with altered GABARAP processing.

FLCN interacts with GABARAP in the presence of FNIP1 and 2 - The FLCN binding partner, FNIP1, was recently shown to interact with GABARAP.[34] Combined with our finding of enhanced GABARAP levels in *FLCN*-deficient cells, we wished to explore this connection further. Unbiased GABARAP interaction mass spectrometry was performed, and we identified eight high-confidence interacting proteins (Fig. 3A), including both FNIP1 and FLCN (FLCN peptide identification shown in Fig. S2A). We confirmed the FLCN-GABARAP interaction using an *in vitro* binding assay and could detect endogenous FLCN interaction with bacterially generated recombinant GABARAP protein (Fig. 3B). FLCN interacted more strongly with GABARAP than LC3B, a member of the other ATG8 subfamily (Fig. 3C), suggesting enhanced specificity for GABARAP family members. Interestingly, the interaction between FLCN and GABARAP *in vivo* in mammalian cells was not detectable unless FNIP1/2 was also present. FNIP2 especially was able to potently enhance the interaction (Fig. 3D). The interaction in mammalian cells was clearly specific for GABARAP, and not LC3B. We further confirmed this stronger interaction of GABARAP to FLCN-FNIP1/2 by using *in vitro* binding assays with recombinant GABARAP protein (Fig. S2B). Immunofluorescence analysis revealed co-localisation of FLCN with GABARAP at punctate

structures when co-expressed with FNIP2 (Fig. 3E). Overall, these data reveal that FLCN/FNIP interacts with the autophagy machinery via GABARAP.

FLCN does not function upstream of ULK1 – ULK1 is a key activator of the autophagy cascade and a known GABARAP interactor.[35] We observed a weak interaction between V5-tagged ULK1 and HA-FLCN (Fig. 4A), which suggests that FLCN might influence autophagy at the level of ULK1. This FLCN-ULK1 interaction was markedly enhanced when ULK1 contained a kinase inactivating mutation (K46I, referred to as kinase-dead). In a reciprocal experiment, immunoprecipitated HA-FLCN similarly showed a more robust interaction with kinase-dead ULK1 (Fig. S3A).

To determine whether this observed FLCN-ULK1 interaction had a cellular function, we analysed whether ULK1 activity could be modulated by *FLCN* knockdown. To do this, we examined the comparative activity of both AMPK and mTORC1, as these signalling pathways are known to impact autophagy through ULK1 phosphorylation.[10-12, 15-17] AMPK activates autophagy via phosphorylation of ULK1 at Ser555,[15] while Ser758 phosphorylation of ULK1 by mTORC1 is inhibitory and appears to modulate ULK1-AMPK interaction.[16,17] Both AMPK and mTORC1 have also been previously linked to FLCN.[27-29, 36] In control HK2 cells, starvation potently induced the phosphorylation of ULK1 at the AMPK-mediated site (Ser555), while growth media induced the phosphorylation of the mTORC1 site (Ser758) (Fig. 4B). Importantly, we did not notice any marked differences in the levels of ULK1 phosphorylation upon *FLCN* knockdown, except a modest elevation in ULK1 phosphorylation at Ser758 under starvation conditions. Through ULK1 kinase assays, we further confirmed that endogenous ULK1 activity was not significantly impacted upon loss of *FLCN* (Fig. 4C).

ULK1 phosphorylates FLCN - Unlike wild-type ULK1, kinase dead ULK1 is predominantly found in a larger 1.2 MDa complex, suggesting that autophosphorylation as well as substrate phosphorylation is necessary for normal interaction dynamics between ULK1 and substrates.[37] As wild-type ULK1 appears

to weakly interact with FLCN compared to kinase-dead ULK1 (Fig. 4A), this transient interaction might be modulated through ULK1 phosphorylation. To determine whether ULK1 phosphorylates FLCN, we [γ-^{32}P]-orthophosphate radiolabelled HEK293 cells expressing HA-FLCN *in vivo* and determined [γ-^{32}P]-incorporation into HA-FLCN in the presence or absence of ULK1. We observed that ULK1 potently induced FLCN phosphorylation *in vivo* (Fig. 5A), implying that ULK1 might function upstream of FLCN. To test whether ULK1 directly phosphorylates FLCN, we performed *in vitro* ULK1 kinase assays towards FLCN and a known ULK1 substrate, ATG13.[10,11] We found that wild-type ULK1 robustly phosphorylated both FLCN and ATG13 *in vitro*, whereas no phosphorylation was detected with kinase dead ULK1 (Fig. 5B). This data reveals that FLCN is directly phosphorylated by ULK1. Through mass spectrometry, we identified multiple ULK1-mediated phosphorylation events towards FLCN in cells. Within the C-terminus of FLCN, we observed three new phosphorylation sites (Ser406, Ser537 and Ser542), which were unique to FLCN when co-expressed with wild-type ULK1 but not kinase dead ULK1 (Fig. 5C and S3B-D). The Ser406 signal was not localised, but the closest alternative candidate phosphorylation site is Ser407, which is not as well conserved between species (Fig. 5C). The other two localised ULK1 sites, Ser537 and Ser542, are well conserved between species (Fig. 5C). Additional ULK1-mediated phosphorylation sites were observed in the linker region of FLCN (Ser316/Thr317), but these residues are poorly conserved amongst species (Fig. S3E). A structural model showing the three best conserved ULK1-mediated phosphorylation sites of FLCN was generated from the recently determined C-terminal crystal structure of FLCN (Fig. 4D).[38] From the crystal structure [PDB Id: 3V42], we observed that all three ULK1 phosphorylation sites are solvent exposed to the surrounding environment, making them accessible for phosphorylation.

ULK1 modulates the FLCN-GABARAP complex – To determine whether FLCN phosphorylation by ULK1 had a functional consequence, we analysed the FLCN-FNIP2-GABARAP complex in the presence of over-expressed ULK1. We found that expression of wild-type ULK1 impaired the interaction of GABARAP with FLCN/FNIP2, whereas this interaction remained intact in the presence of kinase dead

ULK1 (Fig. 6A). In agreement with the literature,[35] ULK1 was also found in the GABARAP immunoprecipitates. In support of the finding that ULK1 modulates the FLCN-GABARAP interaction, knockdown of endogenous ULK1 expression by shRNA under normal growth conditions markedly strengthened the interaction between FLCN/FNIP2 and GABARAP (Fig. 6B). Collectively, this data implies that the kinase activity of ULK1 is required for FLCN/FNIP2 dissociation from GABARAP. To determine whether the three identified phosphorylation sites in FLCN were important for modulating the interaction, we tested the *in vitro* binding of both wild-type and a triple serine-to-alanine FLCN mutant (3A) to bacterially expressed GST-GABARAP or GST-LC3B as bait. Loss of these phosphorylation sites modestly enhanced binding of FLCN to GABARAP and LC3B (Fig. 6C). As observed previously (Fig. 3C), FLCN preferentially bound to GABARAP. However, when we tested the strength of FLCN(3A)-GABARAP binding in mammalian cells, we found that ULK1 expression could still cause disassembly of the complex (data not shown). This suggests that additional ULK1-mediated phosphorylation events (i.e., additional sites within FLCN and/or FNIP2) further regulate formation of the FLCN-FNIP2-GABARAP complex in cells. However, we observed slight impairment in the ability of the FLCN(3A) mutant to drive autophagy in cells, as determined by a modest repression of SQSTM1 expression when compared to wild-type FLCN (Fig. 6D).

Patient tumours show autophagy defects – To determine whether our findings translated to clinical samples, we analysed SQSTM1 protein levels along with the ATG8 family members, GABARAP and LC3, in a BHD patient renal tumour containing two mutated copies of *FLCN* (a c.499C>T mutation (encoding a truncated FLCN mutant, pGln167X) in one allele and deletion of exon 6 in the other allele).[39] We found that SQSTM1 and GABARAP proteins were elevated in both chromophobe and clear cell sections of the tumour when compared to normal control kidney tissue, with slight elevation of LC3 (Fig. 7A). The observation of raised LC3 and SQSTM1 protein levels could indicate a blockage in the autophagic pathway, preventing proper autophagic flux. We next determined whether FLCN mutants exhibited altered association with ULK1 and GABARAP. We tested ULK1 interaction with a panel of

BHD-patient derived mutations (curated in the Leiden Open Variation Database). We discovered that the C-terminal truncating mutations (Y463X and H429X) interacted more avidly with ULK1 than either wild-type FLCN or a BHD patient-derived point mutation, K508R (Fig. 7B). This suggests that the extreme C-terminus of FLCN does not bind directly to ULK1 and may play a role in dissociation from ULK1. In contrast, these truncation mutants of FLCN show impaired binding to GABARAP (Fig. 7C). Additionally, the mutants were not able to repress SQSTM1 levels as efficiently as wild-type FLCN (Fig. 7D). Collectively, our data suggest that FLCN functions as a positive modulator of autophagy, where loss of FLCN impairs basal autophagy, both *in vitro* and in the disease setting.

Discussion

In this study, we discover that FLCN is a new ULK1 substrate, and FLCN phosphorylation by ULK1 modulates the interaction of FLCN-FNIP2 with the autophagy component, GABARAP. Our analysis reveals that multiple residues within FLCN are phosphorylated in an ULK1-dependent manner. We also uncover that FLCN plays a positive role in autophagy, where loss of FLCN leads to impaired autophagic flux.

The binding partners of FLCN, FNIP1 and FNIP2, have previously been connected to B-cell development,[40] autophagy via GABARAP[34] and the induction of apoptosis following DNA-base mispairing.[41] We reveal that FNIP2 (and to a lesser extent FNIP1) enhances FLCN-GABARAP binding, implying that FLCN functions as a complex with FNIP proteins to regulate autophagy. Lack of this functional complex due to *FLCN* mutations in BHD syndrome could explain the impaired autophagy observed in tumour tissue from BHD syndrome patients.

GABARAP subfamily members appear to function downstream of autophagosome membrane elongation in a step coupled to dissociation of the ATG12-ATG5-ATG16L complex[8] and have been hypothesised to

recruit and anchor the ULK1 complex on autophagosomes.[35, 42] ULK1, along with its binding partners, ATG13 and FIP200, contain LC3-interacting region (LIR) motifs which preferentially bind to the GABARAP subfamily of ATG8 proteins.[35, 42] As FLCN appears to have a preference for binding GABARAP over LC3B, it is likely that FLCN modulates autophagy through GABARAP-dependent processes. Additionally, FNIP2 has a potential LIR motif (Fig. S4), while FNIP1 does not, which might explain why FNIP2 further enhances the FLCN-GABARAP interaction.

We detected elevated SQSTM1 protein levels, as well as GABARAP and LC3, in BHD kidney tumours compared with normal kidney tissue. Interestingly, upregulation of SQSTM1 is observed in several cancers, including glioblastoma multiforme,[43] colorectal cancer[44] and hepatocellular carcinomas,[45] while genomic amplification of the *SQSTM1* gene is seen in some clear cell renal cell carcinomas.[31] SQSTM1 is also overabundant in breast cancer,[46] where its expression level correlates with poorer disease-free survival.[47] Similarly, elevated SQSTM1 is associated with poor prognosis in lung cancer patients.[48] It is known that genetic inactivation of *Atg7* in mice leads to SQSTM1 accumulation and generation of ubiquitin-positive inclusions in the liver. This then sequentially leads to accumulation of nuclear Nrf2, enhanced cellular stress and hepatotoxicity.[49] Sustained SQSTM1 expression has also been linked to tumorigenesis via elevated levels of reactive oxygen species and DNA damage[50] in addition to enhanced cellular migration and invasion.[43] A similar mechanism could operate in *FLCN*-deficient kidney cells, whereby inactivation of *FLCN* causes autophagy deficiencies and elevated SQSTM1 levels, and the resulting cellular stress could promote tumour development.

Recently, both SQSTM1 and FLCN have been linked to amino acid sensing through the Rag proteins and mTORC1. SQSTM1 was found to bind the Rag proteins to favour formation of the active Rag heterodimer, thereby helping activate mTORC1 at the lysosome.[51] Three publications have now linked the FLCN/FNIP complex to the Rags at the lysosome, linking FLCN to amino acid-dependent mTORC1 signalling.[27-29] We did not detect substantially altered mTORC1 signalling following *FLCN* loss in our

cell line model under normal or starved conditions, while other publications have found enhanced mTORC1 activity in animal models lacking *FLCN*, at least in certain cell types.[32, 52] It appears that mTORC1 signalling in the context of *FLCN*-deficiency is cell type dependent and can also alter during tumour development in response to accumulation of other genetic mutations.

BHD syndrome has lately been reported to be a ciliopathy,[25] as alteration to FLCN levels can cause changes to the onset of ciliogenesis. Changes in FLCN levels are also associated with disruption of planar cell polarity and dysregulation of the canonical Wnt signalling pathway. As a compromised ability to activate the autophagic response may be an underlying feature in some ciliopathies,[26] it is possible that there is also an association between cilia and autophagy in BHD syndrome. For instance, impaired autophagy could be a contributing factor to ciliary defects and renal cyst formation in BHD syndrome patients.

While our work helps refine our understanding of FLCN by revealing that FLCN interacts with components integral to autophagy, it is important to highlight that FLCN function is not just restricted to autophagy or the lysosome. For instance, FLCN also interacts with p0071 (also known as plakophilin-4) involved in desmosomal and adherens junctions.[53, 54] Additionally, multiple pathways that drive cancer progression can become dysregulated when FLCN expression is lost, including defects in TGFβ-mediated signalling,[55,56] enhanced hypoxia inducible factor activity[57] and TFE3 activity.[58] Therefore, FLCN appears to play a broader 'housekeeping' role in the cell and is likely to be a fundamental player in autophagy and cellular homeostasis outside the disease setting. Although further studies are required, it seems reasonable to assume that impaired autophagy upon loss of FLCN expression contributes in part to cancer progression in BHD patients.

Materials and Methods

Cell Culture - Stable *FLCN* knockdown in HK2 cells was previously described.[25] *Flcn*+/+ and -/- MEF cells were gifted by Prof. Arnim Pause (McGill University, Canada) derived from mice described previously.[32] All cell lines were cultured in DMEM supplemented with 10 % (v/v) foetal calf serum, 100 U/ml penicillin and 100 μg/ml streptomycin (Life Technologies). Lipofectamine 2000 transfection was used unless otherwise stated and performed according to the manufacturer's protocol (Life Technologies). Cells were harvested 24–36 h post-transfection. Experiments were performed under normal growth conditions, unless otherwise stated. For complete starvation, cells were washed twice in phosphate buffered saline (PBS) and incubated in Krebs Ringer buffer (KRB) (20 mM HEPES (pH 7.4), 115 mM NaCl, 5 mM KCl, 10 mM $NaHCO_3$, 2.5 mM $MgCl_2$, 2.5 mM $CaCl_2$) for 4 h.

Plasmids - V5-ULK1 wild-type and kinase dead (K46I) and GST-ATG13 have been described previously.[22] HA-FLCN was generated in the pN3HA backbone (a kind gift from Dr. Sylvia Neumann, The Scripps Research Institute, San Diego, USA) and untagged-FLCN in the pcDNA3.1 vector. GST-FLCN in pDEST27 and V5-FNIP1 in pcDNA3.1/nV5-DEST were generated using the Gateway system (Life Technologies). HA-FNIP1 was a kind gift from Dr. Laura Schmidt (National Institutes of Health, Bethesda, USA) and myc-FNIP2 was a kind gift from Dr. O. Hino (Juntendo University School of Medicine, Tokyo, Japan).[59] HA-SQSTM1 (Plasmid #28027)[60] and ptfLC3 vector (Plasmid #21074)[33] were from Addgene. LC3B and GABARAP (from pDONR[34]) were cloned into pDEST15 (Life Technologies) or pcDNA-HA, respectively. Mutations were introduced using the QuikChange Site-directed mutagenesis kit (Stratagene, Agilent Technologies).

Antibodies - Anti-HA antibody (11867423001) was purchased from Roche. Anti-β-actin (4967), phospho-ULK1 Ser555 (5869) and Ser758 (6888) and total ULK1 (4773) antibodies were from Cell Signaling. Anti-V5 (46-0705) was from Life Technologies. Anti-Myc clone 9E10 antibody (M5546) was from Sigma-Aldrich and anti-GST antibody (05-782) was from Merck Millipore. Anti-FLCN was gifted from

Prof. Arnim Pause (McGill University, Canada). Anti-SQSTM1 (p62) C-terminal antibody (GP62-C/DS-160211) was from Progen Biotechnik GmbH. Anti-LC3 antibody for immunofluorescence and immunohistochemistry was from Novus Biologicals (NB100-2220), for western blotting from Nanotools (0260-100/LC3-2G6). GABARAP antibody (AP1821a) was from Abgent.

shRNA knockdown - JetPEI transfection mixtures containing 2 μg of scrambled shRNA or ULK1 shRNA (MISSION shRNA 1-1064slcl, Sigma) were prepared according to the manufacturer's protocol (Polyplus-transfection) and reverse transfected into HEK293 cells. Following incubation at 37 °C for 24 h, plates were then transfected with V5-FLCN, myc-FNIP2 and HA-GABARAP using the JetPEI protocol (forward transfection) and incubated for a further 28 h prior to lysis.

Immunoprecipitation, GST-pulldown and western blotting - Cells were lysed in BHD lysis buffer (20 mM Tris, 135 mM NaCl, 5 % (v/v) glycerol, 50 mM NaF and 0.1 % (v/v) Triton X-100, pH 7.5 plus protease inhibitors), centrifuged and protein quantified using Bradford reagent (Sigma-Aldrich). Anti-HA and anti-V5 coupled to Protein G-Sepharose beads (GE Healthcare Life Sciences) were used to immunoprecipitate HA and V5-tagged proteins as appropriate. Immunoprecipitates were washed three times in lysis buffer and resuspended in NuPAGE LDS sample buffer (Life Technologies). Samples for GST-pulldown were lysed in Buffer B (40 mM HEPES (pH 7.5), 120 mM NaCl, 1 mM EDTA, 10 mM pyrophosphate, 10 mM β-glycerophosphate, 50 mM NaF, 1.5 mM Na_3VO_4, 0.3% (w/v) CHAPS plus protease inhibitors) and incubated with glutathione-Sepharose beads (GE Healthcare Life Sciences). Beads were washed three times in lysis buffer, and GST-tagged proteins were eluted using 10 mM glutathione. Western blotting was performed as previously described.[22] Blots shown are representative of at least three independent experiments.

ULK1 kinase assay - Cell lysates from nutrient-replete or starved HK2 cells were immunoprecipitated using anti-ULK1 antibody (J.T. Murray, Queen's University, Belfast, UK). Immunocomplexes were

captured using protein G-Sepharose (GE Healthcare Life Sciences), washed three times in Low Salt Buffer (50 mM Tris-Cl (pH 7.5), 1 mM EGTA, 1 mM EDTA, 0.3 % (w/v) CHAPs, 1 mM sodium orthovanadate, 50 mM sodium fluoride, 5 mM sodium pyrophosphate, 0.27 M sucrose, 0.1 % (v/v) 2-mercaptoethanol) and twice in Assay Buffer (20 mM HEPES (pH 7.5), 150 mM NaCl, 0.1 % β-mercaptoethanol, 25 mM β-glycerophosphate, 100 μM orthovanadate). *In vitro* ULK1 kinase assays against GST-FLCN and GST-ATG13 (purified from HEK293 cells), were carried out using immunoprecipitated V5-tagged ULK1. The assay mix of immunoprecipitated ULK1, 10 mM MgAc, substrate (3 μg MBP, GST-FLCN or GST-ATG13 as required) and 100 μM [^{32}P] ATP in Assay Buffer was incubated at 30 °C for 10 min, then quenched with sample buffer (Life Technologies) and subjected to SDS-PAGE. Relative levels of [^{32}P]-incorporation were determined by autoradiography.

Immunofluorescence and image analysis - HK2 cells were transfected with RFP-GFP-LC3 for 24 h, fixed with paraformaldehyde and imaged under oil immersion at 20°C using a Leica TCS SPE confocal laser scanning fluorescence microscope, using Leica software (Leica DMRBE). Confocal images were stacked and merged using ImageJ v1.43 software. Puncta were counted manually across multiple fields of view from >10 cells per condition, over three independent experiments. The proportion of each type of puncta was calculated and plotted. For co-localisation experiments, MDCK cells were transfected with pEGFP-FLCN-WT, myc-FNIP2 and HA-GABARAP using MetaFectene Pro. After 46 h, cells were washed twice in PBS and starved in KRB containing 4.5 g/l glucose. Cells were stained with mouse-anti-HA (Cell Signaling, 2367) and polyclonal FNIP2 antibody directed against AA117-131 of human FNIP2. Secondary antibodies were goat-anti-rabbit-Alexa568 (Life Technologies, A11036) and goat-anti-mouse-Cy5 (Southern Biotech, 1034-15), with DAPI counterstain.

Binding of FLCN to GST-baits - Bacterially expressed GST, GST-LC3B and GST-GABARAP were purified using glutathione beads, washed in BHD lysis buffer and then incubated with lysate from

HEK293 cells transfected with HA-FLCN (WT or 3A), HA-FNIP1 or myc-FNIP2. Beads were washed three times in lysis buffer, and GST-tagged proteins eluted using 10 mM glutathione.

In vivo radiolabelling - Transfected HEK293 cells were incubated in phosphate-free medium containing 0.2 mCi [^{32}P]-orthophosphate (PerkinElmer) for 4 h. These cells were harvested using BHD lysis buffer. HA-FLCN was immunoprecipitated with anti-HA antibody bound to protein G-Dynabeads (Life Technologies) and washed in lysis buffer.

Mass spectrometry - GST-FLCN was purified from HEK293 cells co-expressing wild-type or kinase dead ULK1. Samples were separated by SDS-PAGE and excised bands were subjected to a modified in-gel trypsin digestion procedure.[61] Eluted peptides were subjected to electrospray ionization prior to LTQ-Orbitrap mass spectrometry (Thermo Fisher). Peptide sequences were determined by matching protein or translated nucleotide databases with the acquired fragmentation pattern by Sequest (ThermoFinnigan).[62] Modification of 79.9663 mass units to serine, threonine and tyrosine was included in the database searches to determine phosphopeptides and manually inspected to ensure confidence.

Structural modelling - Crystal structure coordinates used in the current manuscript are as deposited in the protein data bank[38] (PDB Id: 3V42). The model was generated using Pymol.

Immunostaining of patient tumour - Tissue sections were processed using standard methodology.[25] Sections were incubated with antibodies for LC3, GABARAP and p62/SQSTM1 antibody (610832, BD Bioscience) in 3% (w/v) bovine serum albumin overnight at 4 °C.

GABARAP Interaction network - GABARAP interaction mass spectrometry was performed and analysed as described previously,[34] with the exception that autophagy interaction network baits (33 thereof) were stably expressed using the MSCV NTAP system in A549 non-small cell lung carcinoma cell lines.

441

442 *Densitometry and statistical analysis* - Densitometry was performed using ImageJ v1.43 software.
443 Student's t-test or one way ANOVA followed by LSD post-hoc testing (as appropriate) were used for
444 statistical analysis, with $p < 0.05$ taken to be significant.

445

446 **Acknowledgements**

447 Mass spectrometry was performed by Steve Gygi and Ross Tomaino at the Taplin Biological Mass
448 Spectrometry Facility, Harvard Medical School, Boston, USA. This work was supported by the
449 Myrovlytis Trust [to A.R.T., E.A.D., S.S. and R.K.N.]; Association for International Cancer Research
450 [Career Development Fellowship No.06-914/915 to A.R.T, Grant 11-0687 to M.vS., B.J.C. and A.R.T.];
451 National Institute for Social Care and Health Research (Wales Gene Park); FindACure [to A.R.T.],
452 Cancer Research UK Career Development Fellowship [C20685/A12825 to S.W.]; the Deutsche
453 Forschungsgemeinschaft [BE 4685/1-1 to C.B.]; the Dutch Cancer Society KWF [2009-4352 to M.vS and
454 B.J.C.]; the Annadal foundation [to M.vS. and B.J.C.]; GROW School for Oncology and Developmental
455 Biology [to T.C.]; the McClay Trust [to E.R.]; and the British Heart Foundation [to J.T.M.].

456

457

458

459

460

461

462

463

464

465

466

467 **References**

468 1. Choi AM, Ryter SW, Levine B. Autophagy in human health and disease. N Engl J Med 2013; 368:
469 651-62.
470 2. Taneike M, Yamaguchi O, Nakai A, Hikoso S, Takeda T, Mizote I, Oka T, Tamai T, Oyabu J,
471 Murakawa T, et al. Inhibition of autophagy in the heart induces age-related cardiomyopathy. Autophagy
472 2010; 6: 600-6.
473 3. Komatsu M, Waguri S, Chiba T, Murata S, Iwata J, Tanida I, Ueno T, Koike M, Uchiyama Y,
474 Kominami E, et al. Loss of autophagy in the central nervous system causes neurodegeneration in mice.
475 Nature 2006; 441: 880-4.
476 4. Hara T, Nakamura K, Matsui M, Yamamoto A, Nakahara Y, Suzuki-Migishima R, Yokoyama M,
477 Mishima K, Saito I, Okano H, et al. Suppression of basal autophagy in neural cells causes
478 neurodegenerative disease in mice. Nature 2006; 441: 885-9.
479 5. He C, Klionsky D.J. Regulation Mechanisms and Signaling Pathways of Autophagy. Annu Rev Genet
480 2009; 43: 67-93.
481 6. Klionsky DJ, Baehrecke EH, Brumell JH, Chu CT, Codogno P, Cuervo AM, Debnath J, Deretic V,
482 Elazar Z, Eskelinen EL, et al. A comprehensive glossary of autophagy-related molecules and processes
483 (2nd edition). Autophagy 2011; 7: 1273-94.
484 7. Kabeya Y, Mizushima N, Yamamoto A, Oshitani-Okamoto S, Ohsumi Y, Yoshimori T. LC3,
485 GABARAP and GATE16 localize to autophagosomal membrane depending on form-II formation. J Cell
486 Sci 2004; 117: 2805-12.
487 8. Weidberg H, Shvets E, Shpilka T, Shimron F, Shinder V, Elazar Z. LC3 and GATE-16/GABARAP
488 subfamilies are both essential yet act differently in autophagosome biogenesis. EMBO J 2010; 29: 1792-
489 1802.
490 9. Itakura E, Mizushima N. Characterization of autophagosome formation site by a hierarchical analysis
491 of mammalian Atg proteins. Autophagy 2010; 6: 764-76.

492 10. Hosokawa N, Hara T, Kaizuka T, Kishi C, Takamura A, Miura Y, Iemura S, Natsume T, Takehana
493 K, Yamada N, et al. Nutrient-dependent mTORC1 association with the ULK1-Atg13-FIP200 complex
494 required for autophagy. Mol Biol Cell 2009; 20: 1981-91.
495 11. Jung CH, Jun CB, Ro SH, Kim YM, Otto NM, Cao J, Kundu M, Kim DH. ULK-Atg13-FIP200
496 complexes mediate mTOR signaling to the autophagy machinery. Mol Biol Cell 2009; 20: 1992-2003.
497 12. Ganley IG, du Lam H, Wang J, Ding X, Chen S, Jiang X. ULK1.ATG13.FIP200 complex mediates
498 mTOR signaling and is essential for autophagy. J Biol Chem 2009; 284: 12297-305.
499 13. Mercer CA, Kaliappan A, Dennis PB. A novel, human Atg13 binding protein, Atg101, interacts with
500 ULK1 and is essential for macroautophagy. Autophagy 2009; 5: 649-62.
501 14. Dorsey FC, Rose KL, Coenen S, Prater SM, Cavett V, Cleveland JL, Caldwell-Busby J. Mapping the
502 phosphorylation sites of Ulk1. J Proteome Res 2009; 8: 5253-63.
503 15. Egan DF, Shackelford DB, Mihaylova MM, Gelino S, Kohnz RA, Mair W, Vasquez DS, Joshi A,
504 Gwinn DM, Taylor R, et al. Phosphorylation of ULK1 (hATG1) by AMP-activated protein kinase
505 connects energy sensing to mitophagy. Science 2011; 331: 456-61.
506 16. Kim J, Kundu M, Viollet B, Guan KL. AMPK and mTOR regulate autophagy through direct
507 phosphorylation of Ulk1. Nat Cell Biol 2011; 13: 132-41.
508 17. Shang L, Chen S, Du F, Li S, Zhao L, Wang X. Nutrient starvation elicits an acute autophagic
509 response mediated by Ulk1 dephosphorylation and its subsequent dissociation from AMPK. Proc Natl
510 Acad Sci USA 2011; 108: 4788-93.
511 18. Bach M, Larance M, James DE, Ramm G. The serine/threonine kinase ULK1 is a target of multiple
512 phosphorylation events. Biochem J 2011; 440: 283-91.
513 19. Di Bartolomeo S, Corazzari M, Nazio F, Oliverio S, Lisi G, Antonioli M, Pagliarini V, Matteoni S,
514 Fuoco C, Giunta L, et al. The dynamic interaction of AMBRA1 with the dynein motor complex regulates
515 mammalian autophagy. J Cell Biol 2010; 191: 155-68.

20. Papinski D, Schuschnig M, Reiter W, Wilhelm L, Barnes CA, Maiolica A, Hansmann I, Pfaffenwimmer T, Kijanska M, Stoffel I, et al. Early steps in autophagy depend on direct phosphorylation of atg9 by the atg1 kinase. Mol Cell 2013; 53: 471-83.

21. Löffler AS, Alers S, Dieterle AM, Keppeler H, Franz-Wachtel M, Kundu M, Campbell DG, Wesselborg S, Alessi DR, Stork B. Ulk1-mediated phosphorylation of AMPK constitutes a negative regulatory feedback loop. Autophagy 2011; 7: 696-706.

22. Dunlop EA, Hunt DK, Acosta-Jaquez HA, Fingar DC, Tee AR. ULK1 inhibits mTORC1 signaling, promotes multisite Raptor phosphorylation and hinders substrate binding. Autophagy 2011; 7: 737-47.

23. Jung CH, Seo M, Otto NM, Kim DH. ULK1 inhibits the kinase activity of mTORC1 and cell proliferation. Autophagy 2011; 7: 1212-21.

24. Nickerson ML, Warren MB, Toro JR, Matrosova V, Glenn G, Turner ML, Duray P, Merino M, Choyke P, Pavlovich CP, et al. Mutations in a novel gene lead to kidney tumors, lung wall defects, and benign tumors of the hair follicle in patients with the Birt-Hogg-Dubé syndrome. Cancer Cell 2002; 2: 157-64.

25. Luijten MN, Basten SG, Claessens T, Vernooij M, Scott CL, Janssen R, Easton JA, Kamps MA, Vreeburg M, Broers JL, et al. Birt-Hogg-Dube syndrome is a novel ciliopathy. Hum Mol Genet 2013; 22: 4383-97.

26. Pampliega O, Orhon I, Patel B, Sridhar S, Diaz-Carretero A, Beau I, Codogno P, Satir BH, Satir P, Cuervo, AM. Functional interaction between autophagy and ciliogenesis. Nature 2013; 502: 194-200.

27. Petit CS, Roczniak-Ferguson A, Ferguson SM Recruitment of folliculin to lysosomes supports the amino acid-dependent activation of Rag GTPases. J Cell Biol 2013; 202: 1107-22.

28. Tsun Z, Bar-Peled L, Chantranupong L, Zoncu R, Wang T, Kim C, Spooner E, Sabatini DM. The folliculin tumor suppressor is a GAP for the RagC/D GTPases that signal amino acid levels to mTORC1. Mol Cell 2013; 52: 495-505.

29. Martina JA, Diab HI, Lishu L, Jeong-A L, Patange S, Raben N, Puertollano R. The nutrient-responsive transcription factor TFE3 promotes autophagy, lysosomal biogenesis, and clearance of cellular debris. Sci Signal 2014; e-pub ahead of print 21 January 2014; doi:10.1126/scisignal.2004754.

30. Pankiv S, Clausen TH, Lamark T, Brech A, Bruun JA, Outzen H, Overvatn A, Bjorkoy G, Johansen T. p62/SQSTM1 binds directly to Atg8/LC3 to facilitate degradation of ubiquitinated protein aggregates by autophagy. J Biol Chem 2007; 282: 24131-45.

31. Cancer Genome Atlas Research Network. Comprehensive molecular characterization of clear cell renal cell carcinoma. Nature 2013; 499: 43-9.

32. Hudon V, Sabourin S, Dydensborg AB, Kottis V, Ghazi A, Paquet M, Crosby K, Pomerleau V, Uetani N, Pause A. Renal tumour suppressor function of the Birt-Hogg-Dubé syndrome gene product folliculin. J Med Genet 2010; 47: 182-9.

33. Kimura S, Noda T, Yoshimori T. Dissection of the autophagosome maturation process by a novel reporter protein, tandem fluorescent-tagged LC3. Autophagy 2007; 3: 452-60.

34. Behrends C, Sowa ME, Gygi SP, Harper JW. Network organization of the human autophagy system. Nature 2010; 466: 68-76.

35. Alemu EA, Lamark T, Torgersen KM, Birgisdottir AB, Larsen KB, Jain A, Olsvik H, Overvatn A, Kirkin V, Johansen T. ATG8 family proteins act as scaffolds for assembly of the ULK complex: sequence requirements for LC3-interacting region (LIR) motifs. J Biol Chem 2012; 287: 39275-90.

36. Baba M, Hong SB, Sharma N, Warren MB, Nickerson ML, Iwamatsu A, Esposito D, Gillette WK, Hopkins RF, Hartly JL, et al. Folliculin encoded by the BHD gene interacts with a binding protein, FNIP1, and AMPK, and is involved in AMPK and mTOR signaling. Proc Natl Acad Sci USA 2006; 103: 15552-7.

37. Chan EYW, Longatti A, McKnight NC, Tooze SA. Kinase-Inactivated ULK Proteins Inhibit Autophagy via Their Conserved C-Terminal Domains Using an Atg13-Independent Mechanism. Mol Cell Biol 2009; 29: 157–71.

565 38. Nookala RK, Langemeyer L, Pacitto A, Ochoa-Montaño B, Donaldson JC, Blaszczyk BK, Chirgadze
566 DY, Barr FA, Bazan JF, Blundell TL. Crystal structure of folliculin reveals a hidDENN function in
567 genetically inherited renal cancer. Open Biol 2012; 2: 120071.
568 39. Menko FH, Johannesma PC, van Moorselaar RJ, Reinhard R, van Waesberghe JH, Thunnissen E,
569 Houweling AC, Leter EM, Waisfisz Q, van Doorn MB, et al. A de novo FLCN mutation in a patient with
570 spontaneous pneumothorax and renal cancer; a clinical and molecular evaluation. Fam Cancer 2013; 12:
571 373-9.
572 40. Baba M, Keller JR, Sun HW, Resch W, Kuchen S, Suh HC, Hasumi H, Hasumi Y, Kieffer-Kwon KR,
573 Gonzalez CG, et al. The folliculin-FNIP1 pathway deleted in human Birt-Hogg-Dubé syndrome is
574 required for murine B-cell development. Blood 2012; 120: 1254-61.
575 41. Lim TH, Fujikane R, Sano S, Sakagami R, Nakatsu Y, Tsuzuki T, Sekiguchiand M, Hidaka M.
576 Activation of AMP-activated protein kinase by MAPO1 and FLCN induces apoptosis triggered by
577 alkylated base mismatch in DNA. DNA Repair (Amst) 2012; 11: 259-66.
578 42. Kraft C, Kijanska M, Kalie E, Siergiejuk E, Lee SS, Semplicio G, Stoffel I, Brezovich A, Verma M,
579 Hansmann I, et al. Binding of the Atg1/ULK1 kinase to the ubiquitin-like protein Atg8 regulates
580 autophagy. EMBO J 2012; 31: 3691-703.
581 43. Galavotti S, Bartesaghi S, Faccenda D, Shaked-Rabi M, Sanzone S, McEvoy A, Dinsdale D,
582 Condorelli F, Brandner S, Campanella M, et al. The autophagy-associated factors DRAM1 and p62
583 regulate cell migration and invasion in glioblastoma stem cells. Oncogene 2012; 32: 699-712.
584 44. Ren F, Shu G, Liu G, Liu D, Zhou J, Yuan L, Zhou J. Knockdown of p62/sequestosome 1 attenuates
585 autophagy and inhibits colorectal cancer cell growth. Mol Cell Biochem 2014; 385: 95-102.
586 45. Inami Y, Waguri S, Sakamoto A, Kouno T, Nakada K, Hino O, Watanabe S, Ando J, Iwadate M,
587 Yamamoto M, et al. Persistent activation of Nrf2 through p62 in hepatocellular carcinoma cells. J Cell
588 Biol 2011; 193: 275-84.
589 46. Thompson HG, Harris JW, Wold BJ, Lin F, Brody JP. p62 overexpression in breast tumors and
590 regulation by prostate-derived Ets factor in breast cancer cells. Oncogene 2003; 22: 2322-33.

591 47. Luo RZ, Yuan ZY, Li M, Xi SY, Fu J, He J. Accumulation of p62 is associated with poor prognosis in
592 patients with triple-negative breast cancer. Onco Targets Ther 2013; 6: 883-8.
593 48. Inoue D, Suzuki T, Mitsuishi Y, Miki Y, Suzuki S, Sugawara S, Watanabe M, Sakurada A, Endo C,
594 Uruno A, et al. Accumulation of p62/SQSTM1 is associated with poor prognosis in patients with lung
595 adenocarcinoma. Cancer Sci 2012; 103: 760-6.
596 49. Komatsu M, Waguri S, Koike M, Sou Y, Ueno T, Hara T, Mizushima N, Iwata J, Ezaki J, Murata S,
597 et al. Homeostatic levels of p62 control cytoplasmic inclusion body formation in autophagy-deficient
598 mice. Cell 2007; 131: 1149–63.
599 50. Mathew R, Karp CM, Beaudoin B, Vuong N, Chen G, Chen HY, Bray K, Reddy A, Bhanot G,
600 Gelinas C, et al. Autophagy suppresses tumorigenesis through elimination of p62. Cell 2009; 137: 1062-
601 75.
602 51. Duran A, Amanchy R, Linares JF, Joshi J, Abu-Baker S, Porollo A, Hansen M, Moscat J, Diaz-Meco
603 MT. p62 is a key regulator of nutrient sensing in the mTORC1 pathway. Mol Cell 2011; 44: 134-46.
604 52. Hasumi Y, Baba M, Ajima R, Hasumi H, Valera VA, Klein ME, Haines DC, Merino MJ, Hong SB,
605 Yamaguchi TP, et al. Homozygous loss of BHD causes early embryonic lethality and kidney tumor
606 development with activation of mTORC1 and mTORC2. Proc Natl Acad Sci USA 2009; 106: 18722-7.
607 53. Medvetz DA, Khabibullin D, Hariharan V, Ongusaha PP, Goncharova EA, Schlechter T, Darling TN,
608 Hofmann I, Krymskaya VP, Liao JK, et al. Folliculin, the product of the Birt-Hogg-Dube tumor
609 suppressor gene, interacts with the adherens junction protein p0071 to regulate cell-cell adhesion. PLoS
610 One 2012; **7**: e47842.
611 54. Nahorski MS, Seabra L, Straatman-Iwanowska A, Wingenfeld A, Reiman A, Lu X, Klomp JA, Teh
612 BT, Hatzfeld M, Gissen P, et al. Folliculin interacts with p0071 (plakophilin-4) and deficiency is
613 associated with disordered RhoA signalling, epithelial polarization and cytokinesis. Hum Mol Genet
614 2012; 21: 5268-79.

615 55. Hong SB, Oh H, Valera VA, Stull J, Ngo DT, Baba M, Merino MJ, Linehan WM, Schmidt LS.
616 Tumor suppressor FLCN inhibits tumorigenesis of a FLCN-null renal cancer cell line and regulates
617 expression of key molecules in TGF-beta signaling. Mol Cancer 2010; 9: 160.
618 56. Cash TP, Gruber JJ, Hartman TR, Henske EP, Simon MC. Loss of the Birt–Hogg–Dubé tumor
619 suppressor results in apoptotic resistance due to aberrant TGFβ-mediated transcription. Oncogene 2011;
620 30: 2534-46.
621 57. Preston RS, Philp A, Claessens T, Gijezen L, Dydensborg AB, Dunlop EA, Harper KT, Brinkhuizen
622 T, Menko FH, Davies DM, et al. Absence of the Birt-Hogg-Dubé gene product is associated with
623 increased hypoxia-inducible factor transcriptional activity and a loss of metabolic flexibility. Oncogene
624 2011; 30: 1159-73.
625 58. Hong SB, Oh H, Valera VA, Baba M, Schmidt LS, Linehan WM. Inactivation of the FLCN tumor
626 suppressor gene induces TFE3 transcriptional activity by increasing its nuclear localization. PLoS One
627 2010; 5: e15793.
628 59. Takagi Y, Kobayashi T, Shiono M, Wang L, Piao X, Sun G, Zhang D, Abe M, Hagiwara Y,
629 Takahashi K, et al. Interaction of folliculin (Birt-Hogg-Dubé gene product) with a novel Fnip1-like
630 (FnipL/Fnip2) protein. Oncogene 2008; 27: 5339-47.
631 60. Fan W, Tang Z, Chen D, Moughon D, Ding X, Chen S, Zhu M, Zhong Q. Keap1 facilitates p62-
632 mediated ubiquitin aggregate clearance via autophagy. Autophagy 2010; 6: 614-21.
633 61. Shevchenko A, Wilm M, Vorm O, Mann M. Mass spectrometric sequencing of proteins silver-stained
634 polyacrylamide gels. Anal Chem 1996; 68: 850-8.
635 62. Eng JK, McKormack AL, Yates JR. An Approach to Correlate Tandem Mass Spectral Data of
636 Peptides with Amino Acid Sequences in a Protein Database. J Am Soc Mass Spectrom 1994; 5: 976-89.
637
638
639
640

641 **Figure Legends**

642

643 **Figure 1: SQSTM1 levels are elevated in *FLCN*-deficient cells and BHD-tumour derived tissue**

644 (A) Control HK2 cells (non-target (NT) shRNA) and those with stable knockdown of *FLCN* were starved
645 for 4 h in Kreb's Ringer Buffer (KRB) or grown in normal media and SQSTM1 levels were analysed.
646 Data is mean ± S.E.M of 3 independent experiments. (B) HA-FLCN was re-expressed (with co-expressed
647 HA-SQSTM1) in *FLCN* knockdown HK2 cells and HA-SQSTM1 levels were analysed by western blot.
648 Data is mean ± S.E.M of 3 independent experiments. *** $p < 0.001$. (C) A tumour sample (T) showing
649 mixed histology of clear and chromophobe cells, and surrounding normal tissue (N) from a BHD patient
650 was stained for SQSTM1. The scale bar is 100 μm.

651

652 **Figure 2: FLCN is a positive driver of autophagy**

653 (A) HK2 control and *FLCN* knockdown cells were transfected with the ptfLC3 vector, fixed and
654 examined by confocal microscopy. Representative maximal Z‑projection images of cells showing the
655 RFP-GFP-LC3 puncta are shown. Scale bar is 10 μm. Red and yellow puncta were scored across three
656 independent experiments (at least 30 cells per cell line in total) and are plotted in (B) mean ± S.E.M. (C)
657 Control HK2 cells and those with stable knockdown of *FLCN* were treated with 100 μM chloroquine
658 (CQ) for the indicated times. Samples were probed for conversion of LC3B (graphed in panel below,
659 mean ± S.E.M.) and GABARAP expression. (D) As for (C) but in HEK293 cells with transient
660 knockdown of *FLCN* expression. For all graphs * $p < 0.05$, ** $p < 0.01$.

661

662 **Figure 3: FLCN interacts with GABARAP, which is enhanced in the presence of FNIP1/2**

663 (A) A network of GABARAP interactors, as determined by mass spectrometry. (B) GST alone or GST-
664 GABARAP was used as bait, and bound endogenous FLCN was detected by western blot. (C) Bacterially
665 expressed GST, GST-LC3B and GST-GABARAP was used as bait for lysates with or without over-

expression of HA-FLCN. Following GST purification, bound HA-FLCN was detected by western blot. (D) V5-FLCN, HA-LC3B or HA-GABARAP were expressed in HEK293 cells with FNIP proteins where indicated. Following an HA immunoprecipitation, V5-FLCN was detected by western blot. Total blots represent 30 % of IP input. (E) MDCK cells were transfected with EGFP-FLCN-WT, myc-FNIP2 and HA-GABARAP. Cells were stained with mouse-anti-HA and polyclonal FNIP2 antibody. Scale bar is 20 μm.

Figure 4: FLCN interacts with ULK1 but does not alter ULK1 activity

(A) FLCN was co-expressed with V5-tagged wild-type (WT) or kinase dead (KD) ULK1 as indicated in HEK293 cells, and subjected to V5 immunoprecipitation. FLCN bound to ULK1 was detected by western blotting. Total blots represent 40 % of IP input. (B) Control HK2 cells and those with stable knockdown of FLCN were transfected with kinase dead ULK1 for 24 h, followed by starvation for 4 h in KRB where indicated. V5-tagged ULK1 was immunoprecipitated and probed for phosphorylation at Ser555 and Ser758. (C) Endogenous ULK1 activity was measured by incorporation of [^{32}P] into myelin basic protein (MBP). The graph shows relative ULK1 activity across three independent experiments, mean ± S.E.M. NS = not significant, * $p < 0.05$.

Figure 5: ULK1 phosphorylates FLCN

(A) Incorporation of [^{32}P] into HA-FLCN *in vivo* was determined in the presence and absence of ULK1. (B) Both ATG13 and FLCN can be phosphorylated by wild-type (WT) but not kinase dead (KD) ULK1 *in vitro*. (C) A multi-species alignment of FLCN proteins using Clustal Omega shows that the Ser406, Ser537 and Ser542 phosphorylation sites are well conserved between species. (D) Cartoon representation of the mapped phosphorylation sites on the crystal structure of the FLCN C-terminal domain (PDB Id: 3V42). The insets show a closer view of the serine residues, which are represented as sticks.

692 **Figure 6: ULK1 modulates the FLCN-GABARAP interaction**

693 (A) V5-FLCN and myc-FNIP2 bound to HA-GABARAP in the presence or absence of wild-type (WT) or
694 kinase dead (KD) V5-ULK1 were determined by immunoprecipitating HA-GABARAP and detecting
695 bound proteins by western blot. Total blots represent 20% of IP input. (B) Cells were transfected with
696 control or *ULK1* shRNA, along with V5-FLCN, myc-FNIP2 and HA-GABARAP and grown in complete
697 DMEM. Following an HA immunoprecipitation, V5-FLCN and myc-FNIP2 were detected by western
698 blot. Total blots represent 20 % of IP input. The graphs show relative binding of V5-FLCN to HA-
699 GABARAP and myc-FNIP2 to HA-GABARAP as determined by densitometry across four independent
700 experiments, mean ± S.E.M. * $p < 0.05$. (C) Bacterially expressed GST, GST-LC3B or GST-GABARAP
701 was used as bait for lysates containing HA-FLCN (WT or 3A mutant). Following GST purification,
702 bound HA-FLCN was detected by western blot (right panel). GST loading controls are shown in the left-
703 hand panel. (D) Wild-type (WT) FLCN, or the serine-to-alanine (3A) FLCN mutant, were re-expressed in
704 *FLCN*-deficient HK2 cells, along with HA-SQSTM1. HA-SQSTM1 levels were determined by western
705 blot and densitometry of SQSTM1 levels from three independent experiments are plotted in the graph,
706 mean ± S.E.M. * $p < 0.05$, *** $p < 0.001$.

707

708 **Figure 7: Patient tumours and patient-derived *FLCN* mutations show autophagy defects**

709 (A) Kidney tumour tissues from a BHD patient showing mixed histology of clear cell and chromophobe
710 cells, were stained for SQSTM1, GABARAP and LC3 and compared to normal kidney. The scale bar is
711 50 μm. (B) HA-FLCN (wild-type or patient-derived mutants) was co-expressed with V5-tagged wild-type
712 (WT) ULK1 in HEK293 cells, and subjected to V5 immunoprecipitation. FLCN bound to ULK1 was
713 detected by western blotting. Total blots represent 40 % of IP input. (C) HA-GABARAP was co-
714 expressed with untagged-FLCN (wild-type or patient-derived mutants) and myc-FNIP2 in HEK293 cells,
715 and subjected to HA immunoprecipitation. FLCN bound to GABARAP was detected by western blotting.
716 Total blots represent 5 % of IP input. (D) Untagged FLCN (wild-type or mutants) was re-expressed (with

co-expressed HA-SQSTM1) in *FLCN* knockdown HK2 cells and HA-SQSTM1 levels were analysed by western blot. Data is mean ± S.E.M of 5 independent experiments. * $p < 0.05$, ** $p < 0.01$.

Supplementary Figure Legends

Fig. S1: Autophagy is impaired in *Flcn*-deficient MEF cells

(A) FLCN-expressing or deficient MEF cells were given normal growth media or starved in KRB for 4 h. Total cell lysates were analysed for SQSTM1 levels by western blotting. Relative levels were determined by densitometry and are plotted as mean ± S.E.M. for three independent experiments. * $p < 0.05$ (B) *GABARAP* mRNA expression levels in HK2 cells expressing and deficient for *FLCN* were determined by Q-PCR.

Fig. S2: The FLCN/FNIP complex binds to GABARAP

(A) The peptide sequence of the longest isoform of human FLCN is shown. Highlighted are the peptides identified in two technical replicate LC-MS/MS analyses of NTAP-GABARAP immunoprecipitates (first replicate is bold, second replicate is underlined). (B) Bacterially expressed GST-GABARAP was used as bait for lysates containing HA-FLCN with or without FNIP1 or FNIP2, where indicated. Following GST purification, bound HA-FLCN was detected by western blot.

Fig. S3: Mass spectrometry reveals three ULK1-mediated phosphorylation sites on FLCN

(A) HA-FLCN was co-expressed with V5-tagged wild-type (WT) or kinase dead (KD) ULK1 as indicated in HEK293 cells, and subjected to HA immunoprecipitation. ULK1 bound to FLCN was detected by western blotting. (B-D) Mass spectrometry (LC-MS/MS) was used to determine the phosphorylated residues of FLCN co-expressed with ULK1. (E) A multi-species alignment of FLCN proteins using Clustal Omega shows that the potential ULK1-mediated phosphorylation sites, Ser316 and Thr317 are not well conserved.

Fig. S4: FNIP2 contains a potential LIR motif

The canonical LIR motif together with a sequence comparison of LIR motifs identified in ULK1, ATG13 and FIP200, as well as a potential LIR motif within FNIP2.

Figure 1

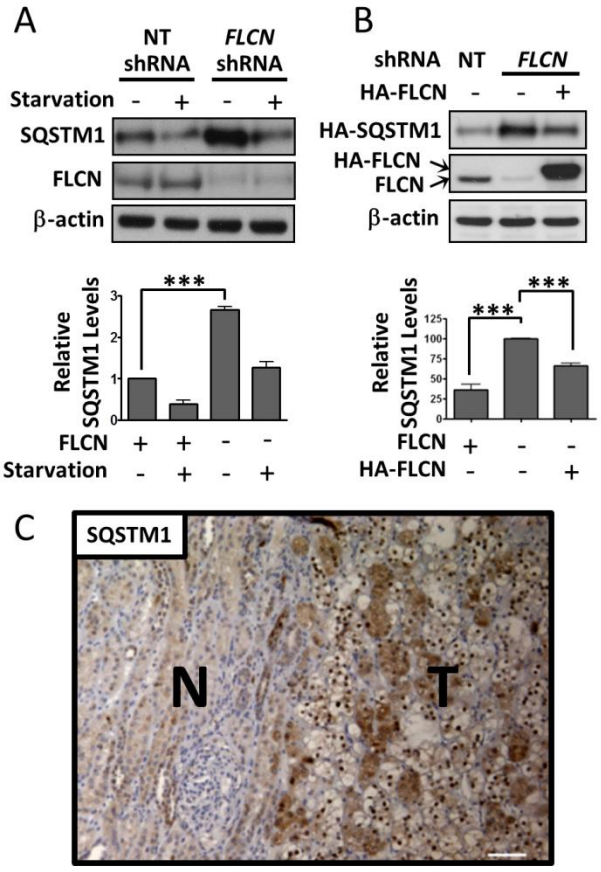
A
NT shRNA
FLCN shRNA
Starvation - + - +
SQSTM1
FLCN
β-actin
Relative SQSTM1 Levels
***
FLCN + + - -
Starvation - + - +
B
shRNA NT FLCN
HA-FLCN - - +
HA-SQSTM1
HA-FLCN
FLCN
β-actin
Relative SQSTM1 Levels
***
***
FLCN + - -
HA-FLCN - - +
C
SQSTM1
N
T

Figure 2

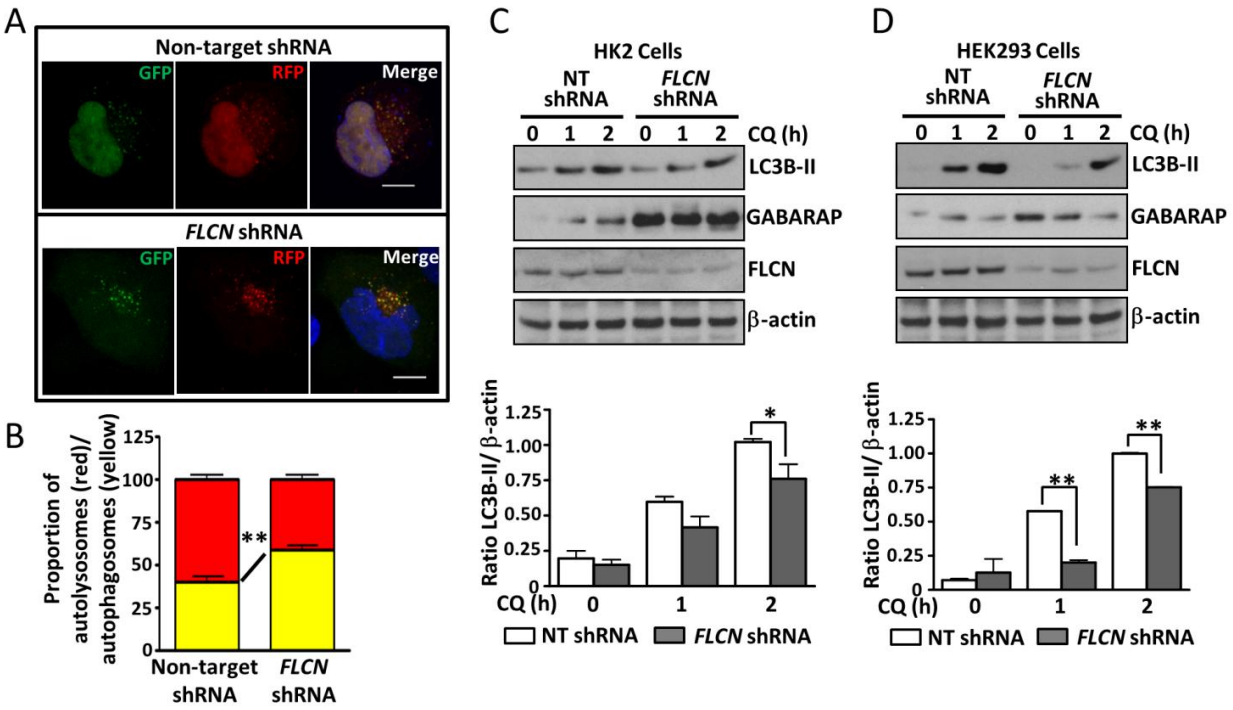
A
Non-target shRNA
GFP
RFP
Merge
FLCN shRNA
GFP
RFP
Merge
B
Proportion of autolysosomes (red)/ autophagosomes (yellow)
125
100
75
50
25
0
**
Non-target shRNA
FLCN shRNA
C
HK2 Cells
NT shRNA
FLCN shRNA
0 1 2 0 1 2 CQ (h)
LC3B-II
GABARAP
FLCN
β-actin
Ratio LC3B-II/ β-actin
1.25
1.00
0.75
0.50
0.25
0
*
CQ (h) 0 1 2
NT shRNA
FLCN shRNA
D
HEK293 Cells
NT shRNA
FLCN shRNA
0 1 2 0 1 2 CQ (h)
LC3B-II
GABARAP
FLCN
β-actin
Ratio LC3B-II/ β-actin
1.25
1.00
0.75
0.50
0.25
0
**
**
CQ (h) 0 1 2
NT shRNA
FLCN shRNA

Figure 3

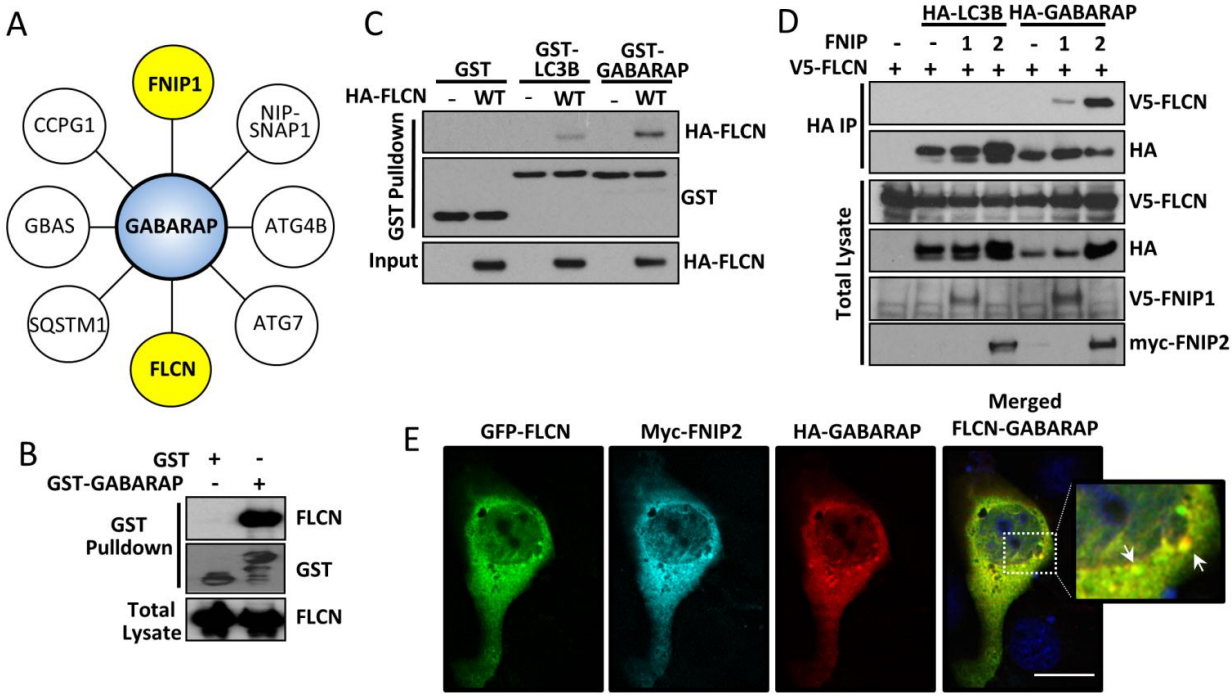
A
FNIP1
CCPG1
NIP-SNAP1
GBAS
GABARAP
ATG4B
SQSTM1
ATG7
FLCN
B
GST + -
GST-GABARAP - +
GST Pulldown
FLCN
GST
Total Lysate
FLCN
C
GST
GST-LC3B
GST-GABARAP
HA-FLCN - WT - WT - WT
GST Pulldown
HA-FLCN
GST
Input
HA-FLCN
D
HA-LC3B HA-GABARAP
FNIP - - 1 2 - 1 2
V5-FLCN + + + + + + +
HA IP
V5-FLCN
HA
Total Lysate
V5-FLCN
HA
V5-FNIP1
myc-FNIP2
E
GFP-FLCN
Myc-FNIP2
HA-GABARAP
Merged FLCN-GABARAP

Figure 4

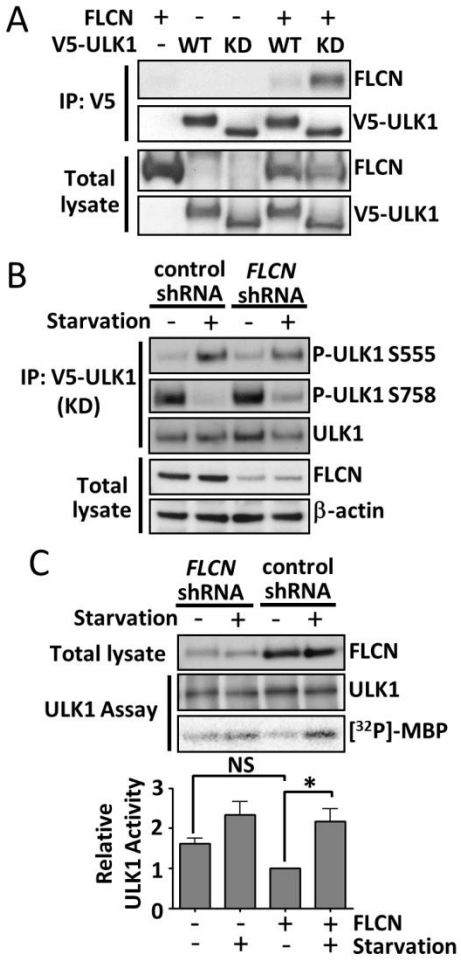
A
FLCN + - - + +
V5-ULK1 - WT KD WT KD
IP: V5
FLCN
V5-ULK1
Total lysate
FLCN
V5-ULK1
B
control shRNA
FLCN shRNA
Starvation - + - +
IP: V5-ULK1 (KD)
P-ULK1 S555
P-ULK1 S758
ULK1
Total lysate
FLCN
β-actin
C
FLCN shRNA
control shRNA
Starvation - + - +
Total lysate
FLCN
ULK1 Assay
ULK1
[32P]-MBP
NS
*
Relative ULK1 Activity
3
2
1
0
- - + + FLCN
- + - + Starvation

Figure 5

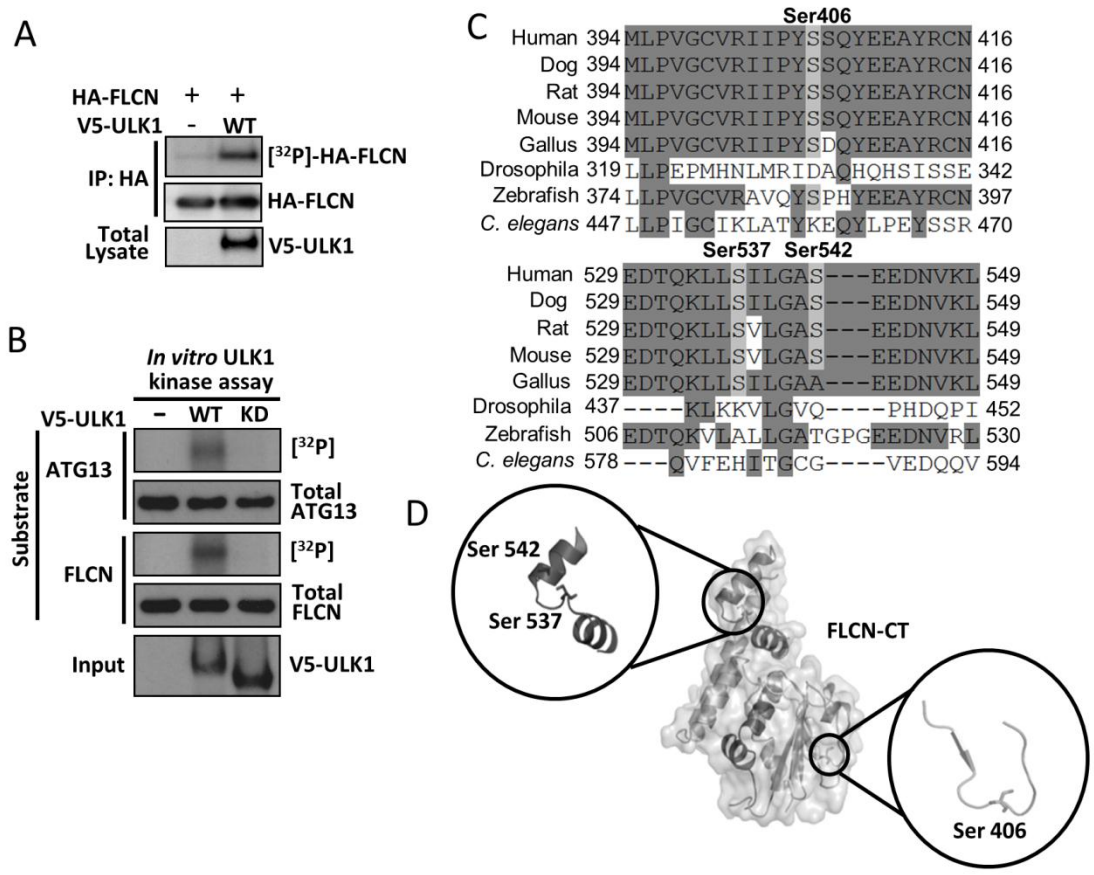
A
HA-FLCN + +
V5-ULK1 - WT
IP: HA
[32P]-HA-FLCN
HA-FLCN
Total Lysate
V5-ULK1
B
In vitro ULK1 kinase assay
V5-ULK1 - WT KD
Substrate
ATG13
[32P]
Total ATG13
FLCN
[32P]
Total FLCN
Input
V5-ULK1
C
Ser406
Human 394 MLPVGCVRIIPYSSQYEEAYRCN 416
Dog 394 MLPVGCVRIIPYSSQYEEAYRCN 416
Rat 394 MLPVGCVRIIPYSSQYEEAYRCN 416
Mouse 394 MLPVGCVRIIPYSSQYEEAYRCN 416
Gallus 394 MLPVGCVRIIPYSDQYEEAYRCN 416
Drosophila 319 LLPEPMHNLMRIDAQHQHSISSE 342
Zebrafish 374 LLPVGCVRAVQYSPHYEEAYRCN 397
C. elegans 447 LLPIGCIKLATYKEQYLPEYSSR 470
Ser537 Ser542
Human 529 EDTQKLLSILGAS---EEDNVKL 549
Dog 529 EDTQKLLSILGAS---EEDNVKL 549
Rat 529 EDTQKLLSVLGAS---EEDNVKL 549
Mouse 529 EDTQKLLSVLGAS---EEDNVKL 549
Gallus 529 EDTQKLLSILGAA---EEDNVKL 549
Drosophila 437 ----KLKKVLGVQ----PHDQPI 452
Zebrafish 506 EDTQKVLALLGATGPGEEDNVRL 530
C. elegans 578 ---QVFEHITGCG----VEDQQV 594
D
Ser 542
Ser 537
FLCN-CT
Ser 406

Figure 6

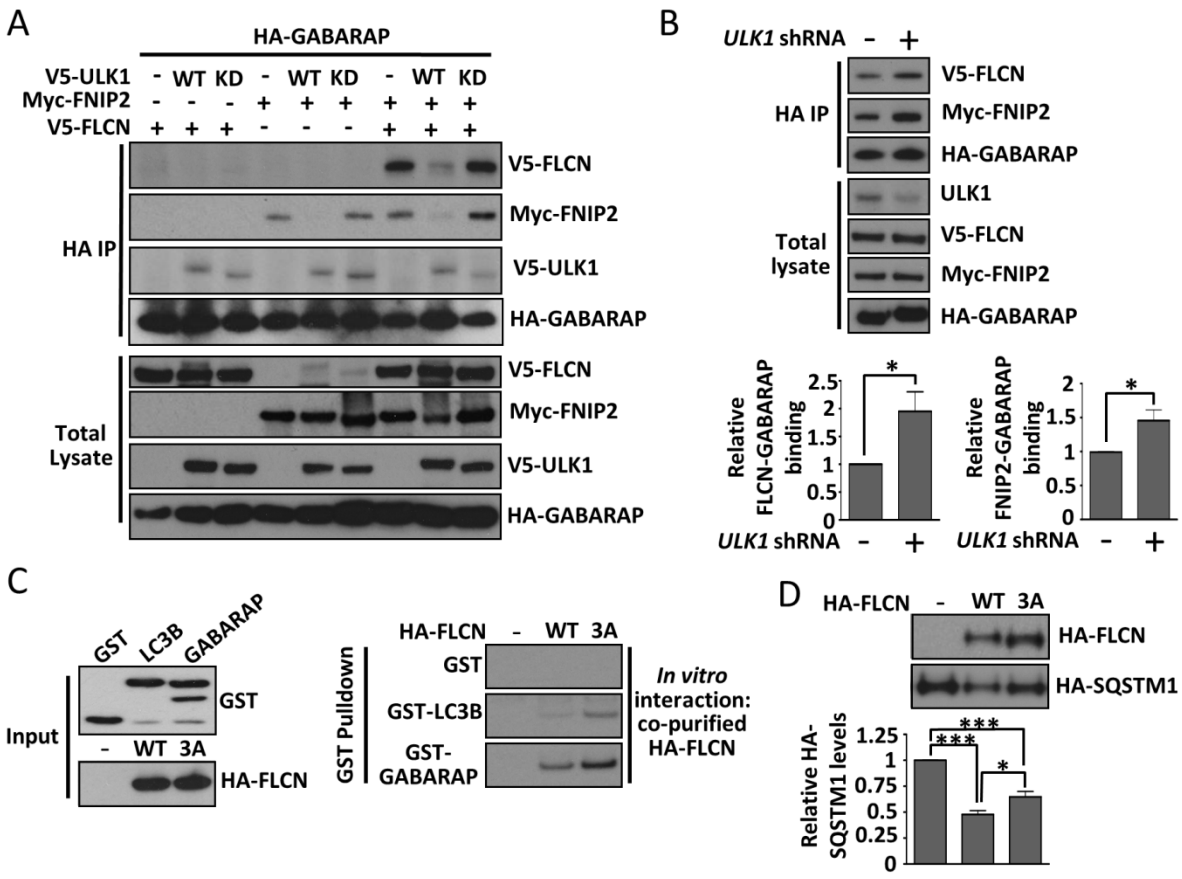
A
HA-GABARAP
V5-ULK1 - WT KD - WT KD - WT KD
Myc-FNIP2 - - - + + + + + +
V5-FLCN + + + - - - + + +
HA IP
V5-FLCN
Myc-FNIP2
V5-ULK1
HA-GABARAP
Total Lysate
V5-FLCN
Myc-FNIP2
V5-ULK1
HA-GABARAP
B
ULK1 shRNA - +
HA IP
V5-FLCN
Myc-FNIP2
HA-GABARAP
Total lysate
ULK1
V5-FLCN
Myc-FNIP2
HA-GABARAP
Relative FLCN-GABARAP binding
2.5
2
1.5
1
0.5
0
*
ULK1 shRNA - +
Relative FNIP2-GABARAP binding
2
1.5
1
0.5
0
*
ULK1 shRNA - +
C
GST LC3B GABARAP
Input
GST
- WT 3A
HA-FLCN
GST Pulldown
HA-FLCN - WT 3A
GST
GST-LC3B
GST-GABARAP
In vitro interaction: co-purified HA-FLCN
D
HA-FLCN - WT 3A
HA-FLCN
HA-SQSTM1
Relative HA-SQSTM1 levels
1.25
1
0.75
0.5
0.25
0
***
***
*

Figure 7

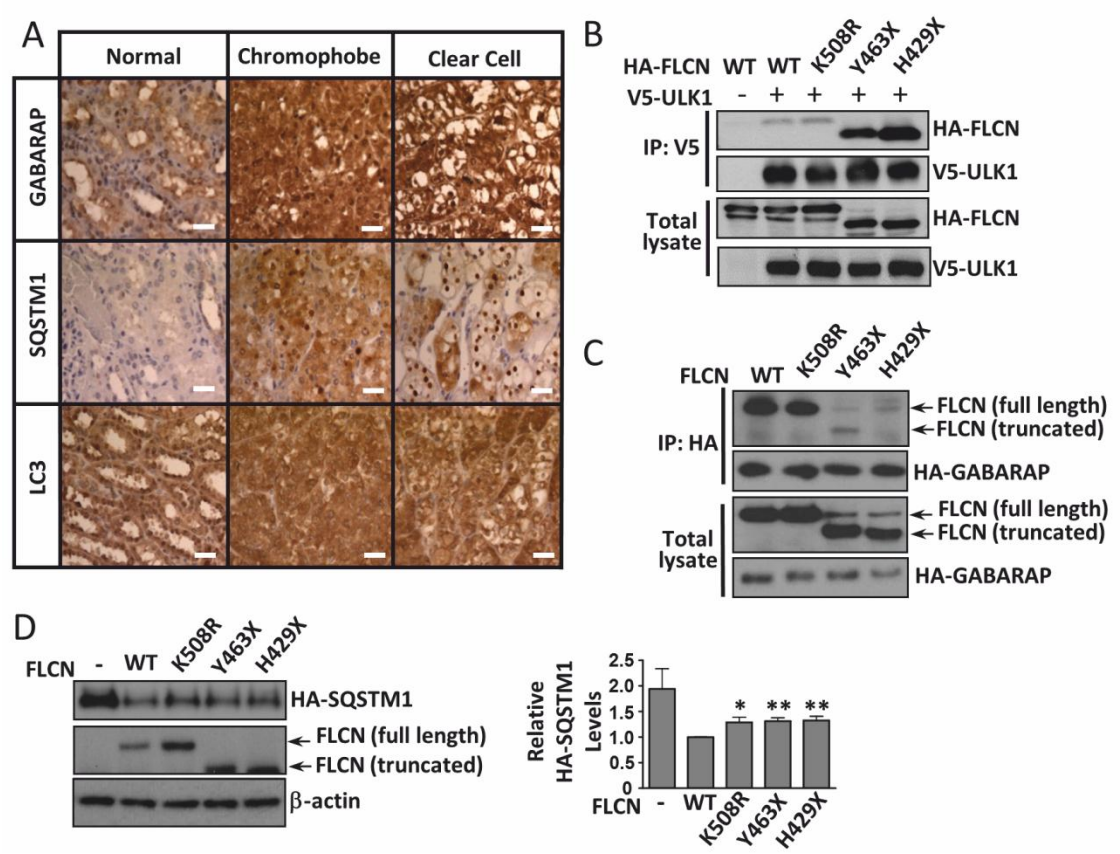
A
Normal
Chromophobe
Clear Cell
GABARAP
SQSTM1
LC3
B
HA-FLCN WT WT K508R Y463X H429X
V5-ULK1 - + + + +
IP: V5
HA-FLCN
V5-ULK1
Total lysate
HA-FLCN
V5-ULK1
C
FLCN WT K508R Y463X H429X
IP: HA
FLCN (full length)
FLCN (truncated)
HA-GABARAP
Total lysate
FLCN (full length)
FLCN (truncated)
HA-GABARAP
D
FLCN - WT K508R Y463X H429X
HA-SQSTM1
FLCN (full length)
FLCN (truncated)
β-actin
Relative HA-SQSTM1 Levels
2.5
2.0
1.5
1.0
0.5
0
* ** **
FLCN - WT K508R Y463X H429X

Supp Figure 1

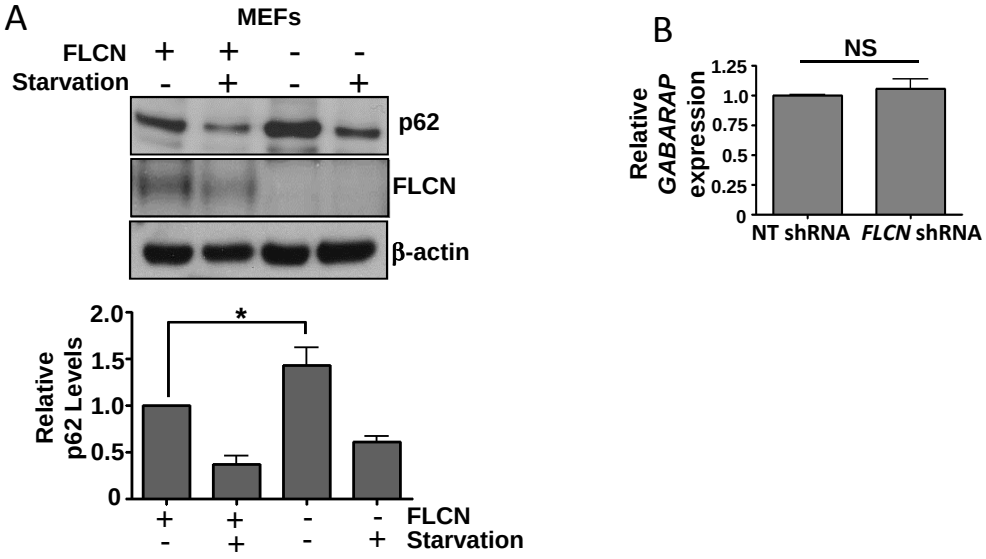

Fig. S1: Autophagy is impaired in *Flcn*-deficient MEF cells

(A) FLCN-expressing or deficient MEF cells were given normal growth media or starved in KRB for 4 h. Total cell lysates were analysed for SQSTM1 levels by western blotting. Relative levels were determined by densitometry and are plotted as mean ± S.E.M. for three independent experiments. * $p < 0.05$ (B) *GABARAP* mRNA expression levels in HK2 cells expressing and deficient for *FLCN* were determined by Q-PCR.

Supp Figure 2

A

MNAIVALCHFCELHGPRTLFCTEVLHAPLPQGDGNEDSPGQGEQAEEEEGGIQMNSRMR**.AHSPAEGASVESS**
SPGPK.KSDMCEGCR.**SLAAGHPGYISHDKETSIK**.YVSHQHPSHPQLFSIVRQACVRSLSCEVCPGREGPIFFGD
EQHGFVFSHTFFIKDSLARGFQRWYSIITIMMDRIYLINSWPFLLGKVRGIIDELQGKALKVFEAEQFGCPQRAQR
MNTAFTPFLHQRNGNAARSLTSLTSDDNLWACLHTSFAWLLKACGSRLTEK**.LLEGAPTEDTLVQMEK**.LADLEE
ESESWDNSEAEEEEKAPVLPESTEGR.ELTQGPAESSSLSGCGSWQPRKLPVFKSLRHMRQVLGAPSFR.MLA
WHVLMGNQVIWK.SRDVDLVQSAFEVLRTMLPVGCVRIIPYSSQYEEAYRCNFLGLSPHVQIPPHVLSSEFAVIVE
VHAAARSTLHPVGCEDDQSLSKYEFVVTSGSPVAADRVGPTILNKIEAALTNQNLSVDVVDQCLVCLKEEWMNK
VKVLFKFTKVDSRPKEDTQKLLSILGASEEDNVKLLKFWMTGLSKTYKSHLMSTVRSPTASESRN

B

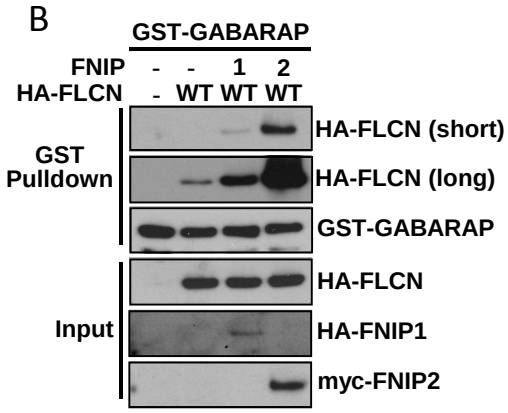

Fig. S2: The FLCN/FNIP complex binds to GABARAP

(A) The peptide sequence of the longest isoform of human FLCN is shown. Highlighted are the peptides identified in two technical replicate LC-MS/MS analyses of NTAP-GABARAP immunoprecipitates (first replicate is bold, second replicate is underlined). (B) Bacterially expressed GST-GABARAP was used as bait for lysates containing HA-FLCN with or without FNIP1 or FNIP2, where indicated. Following GST purification, bound HA-FLCN was detected by western blot.

Supp Figure 3

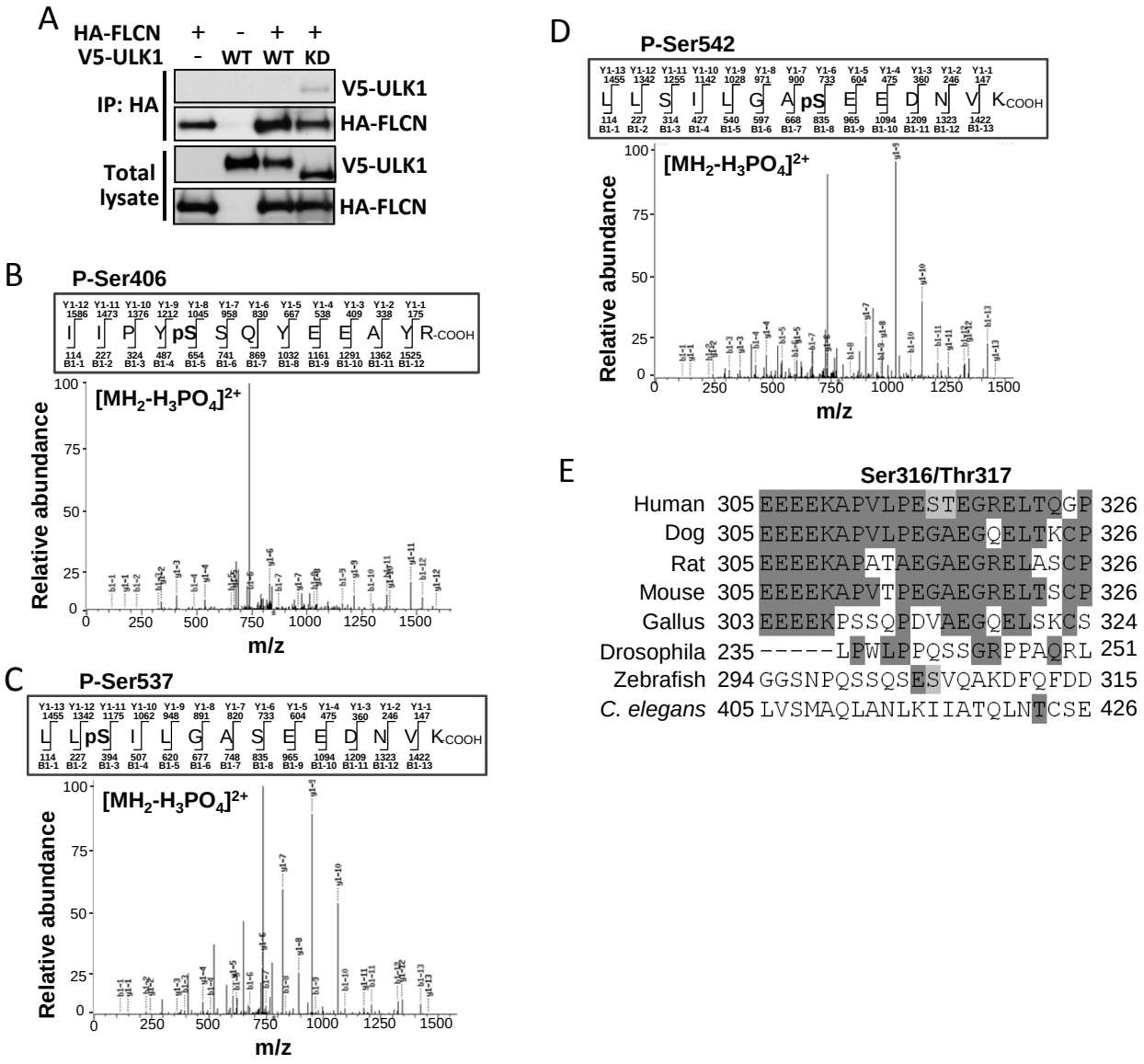

Fig. S3: Mass spectrometry reveals three ULK1-mediated phosphorylation sites on FLCN
(A) HA-FLCN was co-expressed with V5-tagged wild-type (WT) or kinase dead (KD) ULK1 as indicated in HEK293 cells, and subjected to HA immunoprecipitation. ULK1 bound to FLCN was detected by western blotting. (B-D) Mass spectrometry (LC-MS/MS) was used to determine the phosphorylated residues of FLCN co-expressed with ULK1. (E) A multi-species alignment of FLCN proteins using Clustal Omega shows that the potential ULK1-mediated phosphorylation sites, Ser316 and Thr317 are not well conserved.

Supp Figure 4

Fig. S4: FNIP2 contains a potential LIR motif
The canonical LIR motif together with a sequence comparison of LIR motifs identified in ULK1, ATG13 and FIP200, as well as a potential LIR motif within FNIP2.